Non-homogeneous Fabry-Pérot Antenna Design at K_u-band

Pablo Mateos-Ruiz, Elena Abdo-Sánchez, Carlos Camacho-Peñalosa
{pablomr, elenaabdo, ccp}@ic.uma.es
Instituto Universitario de Investigación en Telecomunicación, E.T.S. de Ingeniería de Telecomunicación,
Universidad de Málaga, Andalucía Tech, 29010 Málaga, Spain

***Abstract*—A novel technique to design Fabry-Pérot antennas with non-homogeneous PRS is described. It takes advantage of a transmission line circuit model to efficiently obtain all necessary unit cell designs that satisfy the cavity resonance condition. This approach allows an increase in directivity for a given footprint without decreasing the bandwidth. Some design examples are presented, showing the evolution from a simple single-layer PRS to a non-homogeneous two-layers one. Through electromagnetic simulations, the latter one achieves an increase of about 3 dB in directivity while maintaining the bandwidth. This way, the gain-bandwidth product is improved from a value of 5 to almost 9, effectively raising the antenna efficiency.**

I. Introduction

In recent years, Fabry-Pérot Cavity Antennas (FPCAs) have been greatly studied as an effective technique to increase the directivity of a primary radiation source. This source is placed between two parallel surfaces, one being a ground plane and the other a Partially Reflective Surface (PRS). Trentini [1] was the first to prove the capabilities of these structures, based on Fabry-Pérot resonators and ray theory. These antennas have the advantages of having a low profile, being passive and offering a high directivity with a single feeding point, in contrast to array antennas which require complex feeding networks. However, one of their main drawbacks is their narrow bandwidth, which has attracted a lot of attention in an effort to find ways to solve this problem [2]–[4]. In addition, some works have also focused on dual-band solutions [5], [6], polarization reconfigurability [4] or RCS reduction [7], [8].

The lateral size and how much field is diffracted at the cavity edges are also factors which require further development. Typically, the maximum antenna size has been limited either by available space or computational limitations at simulations. Moreover, as the PRS is more reflective, a larger antenna is commonly needed for the electromagnetic field to be mostly transmitted through the PRS and reduce the lateral radiation. Once the antenna lateral size is fixed, the PRS characteristics can be varied throughout its length in order to better adequate its properties to the field density underneath it, and consequently increasing the antenna efficiency. For example, in [8], a certain degree of heterogeneity is introduced in the PRS design, combining two unit cells with slightly different responses to obtain a more desirable overall performance.

In this article, the PRS non-homogeneity is explored in greater depth as a means of both increasing the bandwidth and directivity. This way, the aim is to better exploit the used space and accomplish a higher antenna efficiency. First, a brief explanation on wide-band PRS unit cell design and modelling is given. After that, a typical homogeneous PRS design is carried out in order to contrast the procedure with a non-homogeneous (NH) design using a novel technique based on the previously explained circuit model. Finally, these designs are simulated and compared to ascertain the improvement in the last one.

II. PRS design

From the simplified ray model, it is derived that, essentially, for a FPCA to work at a desired frequency, the PRS reflection phase ϕ must satisfy the resonance condition given by [1] at that wavelength λ:

$$\phi + \pi - \frac{4\pi}{\lambda} D = 0 \tag{1}$$

being D the cavity height, and assuming that the other reflective surface is a PEC. In addition, the PRS reflection magnitude governs the resonance intensity which, in turn, is proportional to the directivity of the antenna.

On this basis, a simple design can be carried out by simply parameterising any PRS design which allows the adjustment of its reflection magnitude. Once the desired value is achieved, the obtained phase is introduced in (1), thus deriving the necessary cavity height for the antenna to work at the design frequency. This process was already explained in more detail in [9].

However, the PRS design can be further optimised. A common way of doing it is better satisfying the resonance condition around the design frequency, as described in [10]. Rearranging (1), it can be seen that, in order to have maximum directivity within a certain frequency range, the PRS reflection phase must linearly increase with frequency:

$$\phi = \frac{4\pi D}{c} f + (2k-1)\pi, \quad k \in \mathbb{Z}. \tag{2}$$

Consequently, the importance of the PRS design has been a cornerstone around which most of the recent state of the art about FPCAs has mainly focused on. In this way, achieving a positive-gradient reflection phase usually requires the PRS structure to have a (partial) resonance around the design frequency. A more detailed Smith chart-based explanation about the logic behind the positive gradient is given in [2]. From a circuit modelling perspective, at least two components would be necessary for a resonance to be possible. Furthermore, the more degrees of freedom, the better the shaping of the reflection coefficient that can be obtained, but with a more complex design associated.

In this case, a multi-layer approach has been chosen, as it lets the design of each layer to be simpler while facilitating a comprehensive transmission line modelling of the structure.

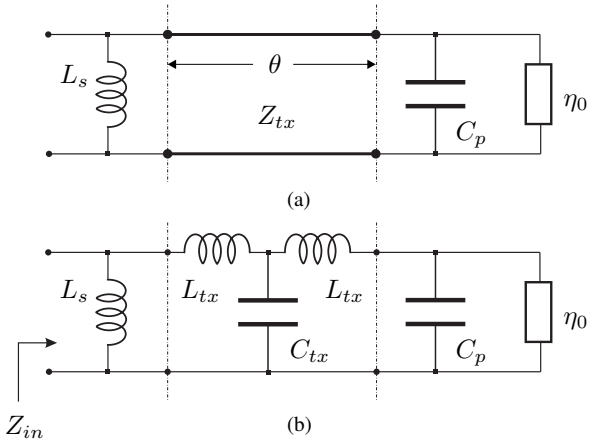

Fig. 1. Transmission Line models: (a) complete and (b) simplified.

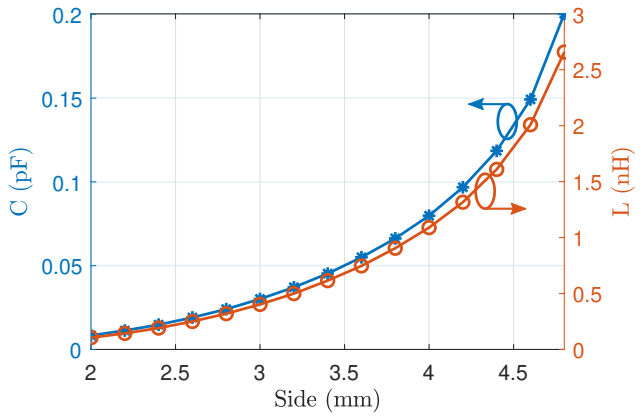

Fig. 2. Equivalent capacitance (left) and inductance (right) values for different side sizes of patch and slot unit cells, respectively, at 14 GHz.

III. Transmission Line Model

In order to synthesize the desired frequency response, a well-known transmission line (TX) model is used to model the multi-layer PRS. In it, each PRS layer is modelled as an impedance in parallel, while the spaces between them are modelled with transmission lines characterised by the length of the gap between both layers and the permittivity of the dielectric used. The vacuum intrinsic impedance must be added after the last layer impedance to account for the air after it. This way, the total reflection coefficient can be obtained from the input impedance of the circuit.

Although any number of layers can be used, only two are selected to illustrate the design procedure. The FPCA design is carried out around 14 GHz, with a complementary design for each of the layers: squared slots for the inner layer and squared patches for the outer one. The periodicity of these unit cells is 5 mm, which is less than $\lambda/4$ at the design frequency, as it must be smaller than the wavelength for them to be seen as homogeneous by the electromagnetic waves.

The patches and slots can be modelled as a capacitance C_p and an inductance L_s in parallel, respectively [3]. Both layers can be assembled from the two sides of a metallized dielectric sheet, making them easier to fabricate. In this design, a RO4350B substrate ($\varepsilon_r = 3.66$) with thickness $h_s = 60$ mils is chosen. This way, the circuit diagram is represented in Fig. 1a, where $\theta = \beta_{tx}\, h_s$ and $Z_{tx} = 120\pi/\varepsilon_r$.

The analytical expression for the input impedance Z_{in} is too complex due to the transmission line. In this sense, as $\theta < 1$, a short transmission line model can be used, which is represented in Fig. 1b. This simplifies the model and allows a relatively compact input impedance expression:

$$Z_{in} = \cfrac{1}{\cfrac{1}{j\omega L_s} + \cfrac{1}{j\omega L_{tx} + \cfrac{1}{j\omega C_{tx} + \cfrac{1}{j\omega L_{tx} + \cfrac{1}{j\omega C_p + \cfrac{1}{\eta_0}}}}}}$$

$$\Gamma_{in} = \frac{Z_{in} - \eta_0}{Z_{in} + \eta_0} \tag{3}$$

where the expressions for the TX inductances and capacitance

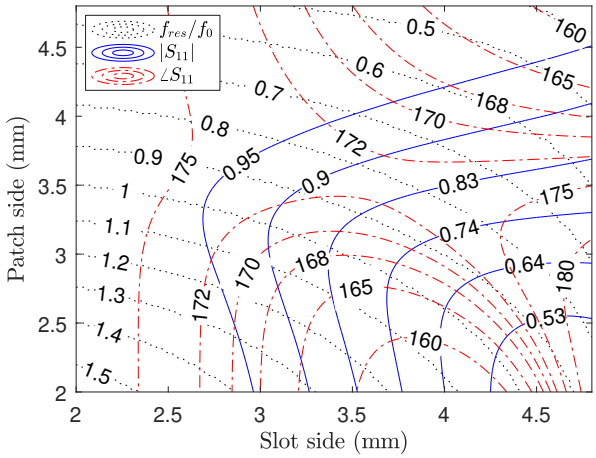

Fig. 3. Reflection magnitude and phase for a mesh of possible PRS designs at $f_0 = 14$ GHz.

are, respectively,

$$L_{tx} = Z_{tx}\sqrt{\mu\varepsilon}\frac{h_s}{2}, \qquad C_{tx} = \frac{\sqrt{\mu\varepsilon}}{Z_{tx}}h_s. \tag{4}$$

As the dielectric length and permittivity are fixed, the two degrees of freedom left reside in the patches and slots reactances. The range of synthesizable values can be obtained varying their sides d_p and d_s through electromagnetic simulations in Ansys HFSS using periodic boundary conditions and Floquet ports. In addition, to account for the substrate next to the layer, the unit cell simulations are carried out with the half-space from the cell to the first port filled with air, and the other one filled with the substrate. The results from these simulations are shown in Fig. 2. It can be seen that both layer unit cells have a very similar response, due to their complementarity.

With these reactance values, all possible designs can be extracted simply using (3) along the desired frequency range. Taking the reflection coefficient (magnitude and phase) at the desired frequency (14 GHz), an isolines diagram can be plotted, as it effectively represents the key values obtained for each design, as can be seen in Fig. 3. In addition, for each design, its normalized resonance frequency (minimum reflection coefficient) respect to the desired frequency is also computed and represented as the third isolines set. This helps

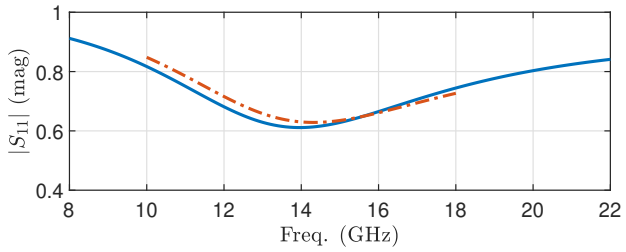

(a) Magnitude.

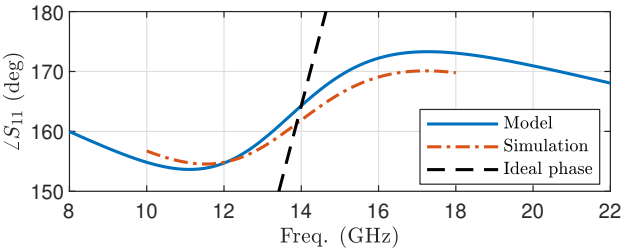

(b) Phase.

Fig. 4. Reflection coefficient for selected homogeneous PRS design.

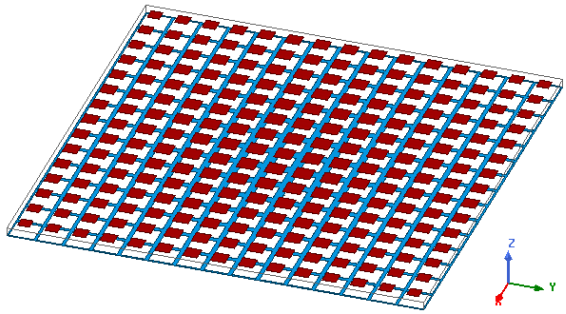

(a) Trimetric view.

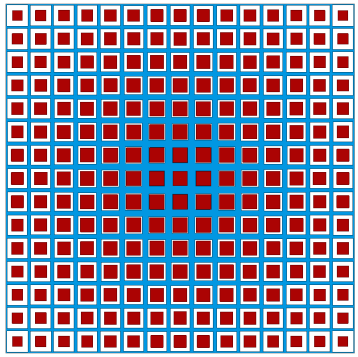

(b) Top view.

Fig. 5. Non-homogeneous Patch-Slots design (v1) overview.

understanding how close to the positive phase gradient the design is.

It is important to note that negligible coupling between the layers must be ascertained for the model to be correct. This can be checked comparing the frequency response of any design extracted with the model and the simulation results of its corresponding complete unit cell.

IV. Design Procedure

A. Homogeneous design

In order to select a particular design, the desired reflection magnitude is determined first. Afterwards, the design along the normalized resonance frequency isoline with unit value would be chosen, as it maximizes the bandwidth. There must be a compromise between how much directivity is wanted and how much the bandwidth can be widen. For this example design, a PRS reflection magnitude of 0.611 is selected, which corresponds with a slot side of $d_s = 4.08\,\mathrm{mm}$ and a patch side of $d_p = 2.52\,\mathrm{mm}$ in order to have the PRS resonance just at $14\,\mathrm{GHz}$. Furthermore, the reflection phase value necessary for obtaining the cavity height in (1) can be directly obtained from Fig. 3. In this case, $\phi = 164.3°$, which gives $D = 10.24\,\mathrm{mm}$.

The frequency response is represented in Fig. 4, where the ideal phase from (2) is also illustrated with a dashed line (Fig. 4b). In addition, the results from the electromagnetic simulation of this design are also shown, proving that the model is accurate enough. The slight discrepancies between the model and the simulations can be explained by the TX line simplification, layers parasitic effects not taken into account in the model, coupling effects between the layers and numerical errors from the simulation. Nevertheless, it can be perfectly used as a base for these designs.

B. Non-homogeneous design

As a type of leaky-wave antenna, FPCAs share the characteristic decaying electromagnetic field along its radiant elements. This effect cause a non-uniform PRS illumination, which translates into a lower aperture efficiency. To solve this problem, leaky-wave antennas tend to present an increasing leakage factor as you move away from the feeder. In this sense, a similar approach can be followed for FPCAs. It has been aforementioned that the resonance condition depends on the phase of the reflection coefficient, and from Fig. 3 a very relevant conclusion can be drawn: it is possible to obtain different reflection magnitudes along the same phase isoline. This way, the resonance condition can be met while decreasing the reflection coefficient of the PRS radially. Consequently, the transmission through it would increase to compensate for the field decay, and achieving a more homogeneous PRS illumination.

For the bandwidth increase effect to be maintained, a proper phase isoline must be selected. Unfortunately, for this unit cell, these isolines do not have a shape that adequately overlaps with the resonance frequency ones. Therefore, the choice of the reflection phase value will depend on which phase isoline is closer to the unit normalised-frequency isoline along the range of desired reflection magnitude values, which will give the bigger phase gradients.

Two similar NH designs are carried out following the previous guidelines. Both present reflection coefficients which decay linearly with the distance from the PRS center, from 0.9 (v1) or 0.95 (v2) at it, to 0.45 at its corner unit cells. For this range of values, the used phase is 170°, since its unit cells resonance frequencies are relatively close to $14\,\mathrm{GHz}$ (Fig. 3). Hence, $D = 10.41\,\mathrm{mm}$ is obtained from (1). In addition, the complete PRS is square-shaped with 15 unit cells of side. An overview of the design v1 is shown in Fig. 5.

V. Simulation Results

First of all, to have a complete comparison, a slots-only PRS is also designed to have a reflection coefficient magni-

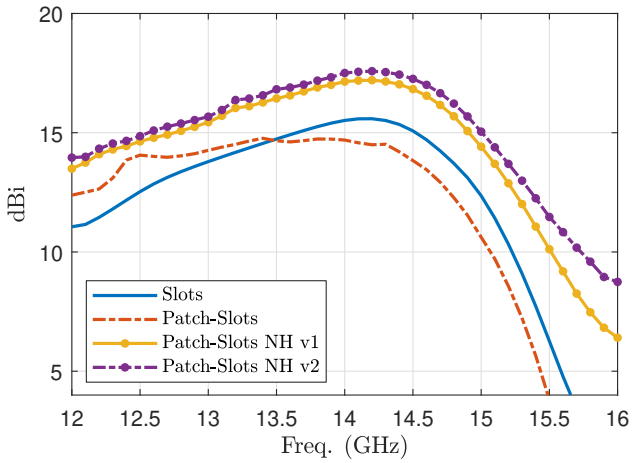

Fig. 6. Simulated directivity at broadside ($\theta = 0°$) for the different designs.

	Slots	**Patch-Slots**	**NH v1**	**NH v2**
ϵ_{ap}	23.5 %	19.5 %	34.1 %	37.2 %
BW	2.45 GHz	$>$ 2.87 GHz	2.78 GHz	2.74 GHz
FBW	17.8 %	$>$ 21.4 %	20.4 %	20.0 %
GBP	5.05	$>$ 5.44	8.25	8.85

TABLE I. FIGURES OF MERIT OF THE DIFFERENT DESIGNS.

tude of around 0.61 (similar to the patch-slots homogeneous design). The slots side used is $d_s = 4.84\,\text{mm}$, the obtained reflection phase is 127.6° and, accordingly, $D = 9.15\,\text{mm}$. This and the designs from subsections IV-A and IV-B are simulated in HFSS using a simple horizontal half-wavelength dipole as the primary source inside the cavity. The dipole has a length of $9.54\,\text{mm}$ and is placed $3.57\,\text{mm}$ above the ground plane parallel to the y-axis, as this configuration is well adapted without a PRS.

The results for the broadside directivity are presented in Fig. 6. All designs effectively have their maximum directivity around 14 GHz. In addition, a clear evolution can be observed from the simpler slot-only to the NH designs. Qualitatively, the homogeneous patch-slots design achieves a greater bandwidth (extends below 12 GHz) than the slots-only one, having a more constant directivity over a wider frequency range, thanks to the positive phase gradient technique. Incorporating the non-homogeneity, the increment in the directivity is significant, taking into account that the bandwidth has not experimented a detrimental effect with respect to the slot-only design, but even a slightly improvement.

Regarding specific figures of merit, in Table I some numerical values are shown, such as aperture efficiency (ϵ_{ap}), half-power bandwidth (BW), fractional bandwidth (FBW) and gain-bandwidth product (GBP), which is defined as follows:

$$\text{GBP} = \frac{\int_{f_L}^{f_U} G(f)\,df}{f_U - f_L}\left(\frac{f_U - f_L}{f_C}\right) = G_{AVG}\,\text{FBW} \qquad (5)$$

The improvement in the GBP of the NH designs is noticeable, as a higher directivity has been achieved without worsening the BW. Furthermore, as the v2 design has a higher starting reflection magnitude, it achieves a slightly better directivity as expected. Of course, these designs could achieve even greater directivity values making the PRS bigger, thus having smaller lateral lobes. However, the main focus in this study is how to exploit the same PRS size to obtain higher aperture efficiencies.

VI. CONCLUSIONS

A comprehensive process to design non-homogeneous FP-CAs in order to increase the aperture efficiency has been presented in this contribution. Moreover, the positive phase gradient technique has been proven to successfully widen the BW, having clearly shown the evolutionary process from a single layer PRS to a NH multi-layer one.

On the other hand, in order to obtain greater bandwidths, several points regarding the unit cell design could be further studied. These would include achieving higher quality factors in order to better satisfy the resonance condition over a wider frequency range, and trying different geometries which may have a better overlapping between their phase and resonance frequency isolines. Although the optimum reflection decay to obtain maximum efficiency is still to be studied, simply using a linear decay with reasonable bounds has already increased the maximum directivity in almost 3 dB, proving the potential of this technique, which resembles metasurfaces design.

As immediate future work, a realistic primary radiation source should be designed and adapted. The latter can be achieved in a computationally efficient way using impedance layer conditions in HFSS. Finally, a design should be fabricated and measured in real conditions.

ACKNOWLEDGEMENTS

This work has been supported by the Spanish Ministerio de Ciencia, Innovación y Universidades (MCIU) (Contrato Juan de la Cierva-Incorporación) under Grant IJC2018-038440-I and by the MCIU/AEI/FEDER (Programa Estatal de I+D+i Orientada a los Retos de la Sociedad) under grant RTI2018-097098-J-I00.

REFERENCES

[1] G. V. Trentini, "Partially reflecting sheet arrays," *IRE Transactions on Antennas and Propagation*, vol. 4, no. 4, pp. 666–671, October 1956.

[2] F. Qin, S. Gao, G. Wei, Q. Luo, C. Mao, C. Gu, J. Xu, and J. Li, "Wideband circularly polarized Fabry-Perot antenna," *IEEE Antennas and Propagation Magazine*, vol. 57, no. 5, pp. 127–135, 2015.

[3] N. Wang, Q. Liu, C. Wu, L. Talbi, Q. Zeng, and J. Xu, "Wideband Fabry-Perot Resonator antenna with two complementary FSS layers," *IEEE Transactions on Antennas and Propagation*, vol. 62, no. 5, pp. 2463–2471, 2014.

[4] R. Lian, Z. Tang, and Y. Yin, "Design of a broadband polarization-reconfigurable Fabry–Perot resonator antenna," *IEEE Antennas and Wireless Propagation Letters*, vol. 17, no. 1, pp. 122–125, 2018.

[5] M. L. Abdelghani, H. Attia, and T. A. Denidni, "Dual- and wideband Fabry–Pérot resonator antenna for WLAN applications," *IEEE Antennas and Wireless Propagation Letters*, vol. 16, pp. 473–476, 2017.

[6] Y.-H. Lv, X. Ding, and B.-Z. Wang, "Dual-wideband high-gain Fabry-Perot cavity antenna," *IEEE Access*, vol. 8, pp. 4754–4760, 2020.

[7] L. Zhang, X. Wan, S. Liu, J. Y. Yin, Q. Zhang, H. T. Wu, and T. J. Cui, "Realization of low scattering for a high-gain Fabry–Perot antenna using coding metasurface," *IEEE Transactions on Antennas and Propagation*, vol. 65, no. 7, pp. 3374–3383, 2017.

[8] Z. Liu, S. Liu, X. Zhao, X. Kong, Z. Huang, and B. Bian, "Wideband gain enhancement and RCS reduction of Fabry–Perot antenna using hybrid reflection method," *IEEE Transactions on Antennas and Propagation*, vol. 68, no. 9, pp. 6497–6505, 2020.

[9] P. Mateos-Ruiz, A. Hernández-Escobar, E. Abdo-Sánchez, and C. Camacho-Peñalosa, "Design and fabrication of a Fabry-Pérot cavity antenna for the Ku-band," in *URSI Málaga*, 2020.

[10] A. P. Feresidis and J. C. Vardaxoglou, "High gain planar antenna using optimised partially reflective surfaces," *IEE Proceedings - Microwaves, Antennas and Propagation*, vol. 148, no. 6, pp. 345–350, Dec 2001.